Title

Right ventricular nitric oxide signaling in an ovine model of congenital heart disease: a preserved fetal phenotype

Journal

AJP Heart and Circulatory Physiology, 309(1)

ISSN

0363-6135

Authors

Kameny, Rebecca Johnson
He, Youping
Morris, Catherine
et al.

Publication Date

2015-07-01

DOI

10.1152/ajpheart.00103.2015

Peer reviewed

Am J Physiol Heart Circ Physiol 309: H157–H165, 2015.
First published May 1, 2015; doi:10.1152/ajpheart.00103.2015.

Right ventricular nitric oxide signaling in an ovine model of congenital heart disease: a preserved fetal phenotype

Rebecca Johnson Kameny,[1,2] Youping He,[3] Catherine Morris,[1] Christine Sun,[1] Michael Johengen,[1] Wenhui Gong,[1] Gary W. Raff,[4] Sanjeev A. Datar,[1] Peter E. Oishi,[1,2] and Jeffrey R. Fineman[1,2]

[1]*Department of Pediatrics, University of California, San Francisco, San Francisco, California;* [2]*Cardiovascular Research Institute, University of California, San Francisco, San Francisco, California;* [3]*Department of Surgery, University of California, San Francisco, San Francisco, California; and* [4]*Department of Surgery, University of California, Davis, Davis, California*

Submitted 10 February 2015; accepted in final form 10 April 2015

Kameny RJ, He Y, Morris C, Sun C, Johengen M, Gong W, Raff GW, Datar SA, Oishi PE, Fineman JR. Right ventricular nitric oxide signaling in an ovine model of congenital heart disease: a preserved fetal phenotype. *Am J Physiol Heart Circ Physiol* 309: H157–H165, 2015. First published May 1, 2015; doi:10.1152/ajpheart.00103.2015.—We recently reported superior right ventricle (RV) performance in response to acute afterload challenge in lambs with a model of congenital heart disease with chronic left-to-right cardiac shunts. Compared with control animals, shunt lambs demonstrated increased contractility because of an enhanced Anrep effect (the slow increase in contractility following myocyte stretch). This advantageous physiological response may reflect preservation of a fetal phenotype, since the RV of shunt lambs remains exposed to increased pressure postnatally. Nitric oxide (NO) production by NO synthase (NOS) is activated by myocyte stretch and is a necessary intermediary of the Anrep response. The purpose of this study was to test the hypothesis that NO signaling is increased in the RV of fetal lambs compared with controls and shunt lambs have persistence of this fetal pattern. An 8-mm graft was placed between the pulmonary artery and aorta in fetal lambs (shunt). NOS isoform expression, activity, and association with activating cofactors were determined in fetal tissue obtained during late-gestation and in 4-wk-old juvenile shunt and control lambs. We demonstrated increased RNA and protein expression of NOS isoforms and increased total NOS activity in the RV of both shunt and fetal lambs compared with control. We also found increased NOS activation and association with cofactors in shunt and fetal RV compared with control. These data demonstrate preserved fetal NOS phenotype and NO signaling in shunt RV, which may partially explain the mechanism underlying the adaptive response to increased afterload seen in the RV of shunt lambs.

right ventricle; Anrep effect

PATIENTS WITH PULMONARY HYPERTENSION (PH) secondary to congenital heart disease (CHD) have improved functional ability and prolonged survival compared with patients with PH resulting from other causes (15, 22). One possible explanation for these observations is that the right ventricle (RV) in patients with PH associated with CHD is uniquely able to respond to the increased afterload created by pulmonary vascular disease (17). For example, the RV in CHD is continually exposed to either increased pressure, volume, or both, potentially altering the normal perinatal transition of the RV from the dominant ventricle in fetal circulation to a low-resistance, high-capacity chamber in postnatal circulation. Given these physiological perturbations, we hypothesized that the RV in CHD has a preserved fetal phenotype that confers an enhanced functional ability to respond to increased afterload.

In our model of CHD with chronic left-to-right shunting, we previously demonstrated that the RV of shunt lambs has an adaptive response compared with control RV when challenged with an acute afterload increase (imposed by pulmonary artery banding), with increased contractility and preservation of mechanical efficiency and ventriculovascular coupling (19). Our observation in the shunt RV of a sustained increase in contractility following afterload challenge is consistent with the Anrep effect, the second slow increase in contractility in response to myocyte stretch (10). Before our report, this critical physiological mechanism had only been observed in the left ventricle (LV), since the normal RV is exquisitely sensitive to increased afterload.

Nitric oxide (NO) signaling has been demonstrated as a critical mediator of excitation-contraction coupling and the slow force response (the in vitro equivalent of the Anrep effect). For example, in single myocyte experiments, Petroff and colleagues demonstrated that NO produced by endothelial NO synthase (eNOS) is a necessary mediator of increased Ca^{2+} release in response to stretch (26). In contrast, Jian and colleagues found neuronal NOS (nNOS), rather than eNOS, to be the critical NOS isoform for intracellular Ca^{2+} release after myocyte stretch (18). The theoretical link between myocyte stretch and intracellular Ca^{2+} release, or mechanochemotransduction, is the result of subcellular compartmentalization of NO production at the sarcoplasmic reticulum (SR), which allows for NO-mediated regulation of Ca^{2+} handling (29).

Therefore, the purpose of the present study was to test the hypothesis that nitric oxide synthase (NOS) activity and its associated signaling are increased in the RV of shunt lambs compared with controls, and this increased NOS signaling in the shunt RV mirrors RV fetal expression and activity. To this end, we used our established, clinically relevant lamb model of a congenital cardiac defect with a large left-to-right shunt, created by the in utero placement of an 8-mm aorta-to-pulmonary shunt (shunt lambs). We examined NOS isoform expression and activity, association with important cofactors, and activating signals in 4-wk-old control and shunt lamb LV and RV tissue and compared these elements with expression in fetal LV and RV.

MATERIALS AND METHODS

Surgical preparation and hemodynamics. A total of six pregnant mixed-breed Western ewes (137–141 days gestation, term = 145 days) were anesthetized. Fetal exposure was obtained through the

Address for reprint requests and other correspondence: J. R. Fineman, Univ. of California, San Francisco, 505 Parnassus Ave., Box 0106, Rm. M-680, San Francisco, CA 94143 (e-mail: jeff.fineman@ucsf.edu).

Table 1. *Quantitative PCR primers*

Target Gene Name	Forward Primer	Reverse Primer
eNOS	gaggggctgtcattccacta	aggggtcttccagatggact
nNOS	accagttggtgaaggtggag	tactcctgcagacccttgct
iNOS	tgttcagctgtgccttcaac	ccggaacttgttggtgagtt
Akt	aacttctctgtggcccaatg	gtctcctcctcctgcctctt
18S	ggatgcgtgcatttatcaga	cttggatgtggtagccgttt

eNOS, endothelial nitric oxide synthase; nNOS, neuronal nitric oxide synthase; iNOS, inducible nitric oxide synthase; Akt, protein kinase B.

horn of the uterus; a left lateral thoracotomy was performed on the fetal lamb. With the use of side biting vascular clamps, an 8.0-mm vascular graft was anastomosed between the ascending aorta and main pulmonary artery of the fetal lambs. This procedure was previously described in detail (27). Control lambs were either provided by twin gestation ($n = 3$) or age matched ($n = 2$). Control lambs did not undergo a lateral thoracotomy. LV and RV tissue was harvested, and hemodynamic measurements were performed when control and shunt lambs were 4 to 5 wk old. Fetal tissue was harvested from late-gestation fetal lambs at the same gestational age as fetal surgery, 137–141 days gestation.

At the time of hemodynamic study, lambs were anesthetized, and catheters were placed in the right and left atrium, main pulmonary artery, and femoral artery (as previously described) (27). An ultrasonic flow probe (Transonics Sytems, Ithaca, NY) was placed around the left pulmonary artery to measure pulmonary blood flow.

At the end of the protocol, all lambs were killed with a lethal injection of pentobarbital sodium (150 mg/kg) followed by bilateral thoracotomy as described in the National Institutes of Health (NIH) *Guidelines for the Care and Use of Laboratory Animals*. The Committee on Animal Research of the University of California, San Francisco, approved all protocols and procedures.

Quantitative real-time PCR. RNA extraction from sheep hearts was performed using a Qiagen RNeasy Fibrous Tissue Mini Kit (Qiagen, Toronto, ON) with the manufacturer's protocols. Identical amounts of purified total RNA were used as starting material. First-strand cDNA was synthesized from each sample and subjected to reverse transcription using the Clontech RNA to cDNA ecoDry Premix (Oligo dT) Kit (Clontech Laboratories) with the manufacturer's protocol.

cDNA templates were mixed with gene-specific primers and Fast-Start Universal SYBR Green Master with Rox reference dye (Roche Applied Science). Primers (Table 1) were designed with public OligoPerfect Designer software (Life Technologies). GAPDH was used as the internal control. The qPCR reactions were completed with an iCycler iQ Real-Time PCR Detection System (Bio-Rad) and always in triplicate. Relative expression levels of genes were analyzed. Differences in cycle threshold number (C_T) were calculated by normalizing the sample cycle threshold of the targeted gene with that of the internal control reference gene 18S. The $\Delta\Delta C_T$ (calculated as $C_{T[target]} - C_{T[reference]}$) method was used to determine relative abundance of expression, as described previously (21).

Immunohistochemistry. Sections from RV and LV of control and shunt juvenile lambs were fixed and prepared for immunohistochemistry staining as previously described (3). Next, tissue sections were incubated with antimyosin heavy chain (MF-20) (Developmental Studies Hybridoma Bank) antibody and anti-eNOS, -nNOS, or -iNOS (all Santa Cruz Biotechnology) antibody in blocking solution at 4°C overnight. After three washes with PBS for 5 min, samples were hybridized with florescent Green 488 goat antirabbit polyclonal and florescent Red 555 goat antimouse monoclonal secondary antibodies (Molecular Probes) at a concentration of 1:500 in blocking solution for 60 min at room temperature. After three further washes with PBS, the slides were mounted with mounting solution with 4′,6-diamidino-2-phenylindole.

Images were taken with a Hamamatsu c10600 ORCA-R2 Digital Camera on a Zeiss Axio Imager Z2 using a ×10 DIC objective and the X-cite 120 Mercury/Halide system and then analyzed using ZEN pro 2012 software (Carl Zeiss Microimaging, Thornwood, NY). All images were subsequently processed using Adobe Photoshop CS5 software (Adobe, San Jose, CA).

Western blot and densitometry analysis. Protein determinations were performed by Western blot analysis as previously described (2). Primary antibodies against eNOS (Santa Cruz Biotech), phospho-eNOS-serine-1177 (Cell Signaling), nNOS (Santa Cruz Biotech), inducible NOS (iNOS) (Santa Cruz Biotech), calmodulin (Santa Cruz Biotech), 90-kDa heat shock protein (hsp90) (polyclonal; BD Transduction laboratories), Akt (Santa Cruz Biotech), phospho-Akt (Santa Cruz Biotech), ryanodine receptor 2 (RyR2) (Affinity Bioreagents), and *S*-nitrosocysteine (Abcam) were used. Anti-β-actin was used as the reference protein for loading controls. Quantification of protein band density in X-ray films from ECL Western blots was performed by the public domain Java image-processing program Image J (NIH Image).

Immunoprecipitation. RV and LV protein was isolated from control, shunt, and fetal hearts, and an equal amount of protein was used in each experiment. Specific antibodies were cross-linked with Protein A/G magnetic beads based on the manufacturer's instructions (Pierce crosslink Immunoprecipitation Kit; Thermo Scientific, Rockford, IL). Protein extracts were incubated with immunoprecipitated (IP) antibody/protein A/G magnetic beads overnight at 4°C. The antigen-antibody beads were next washed two times with IP Lysis/Wash Buffer. Finally, the antigen/antibody complexes were eluted and used for Western blot.

Isolation of SR membrane vesicles. Cardiac SR vesicles were isolated from heart according to Buck et al. (8). Briefly, LV and RV tissue were homogenized in five volumes of homogenization buffer (1 M KCl and 10 mM Tris-maleate, pH 7.0) and a cocktail of protease inhibitors (Roche Applied Science). The homogenate was centrifuged for 20 min at 10,000 *g* at 4°C. The supernatant was discarded, and the remaining pellet was homogenized in an ice-cold homogenization buffer and then centrifuged for 20 min at 6,000 *g* at 4°C. The supernatant from this step was again centrifuged for 25 min at 24,000 *g* at 4°C, and the resulting supernatant was further centrifuged for 120 min at 41,000 *g* at 4°C. The final pellet was resuspended in buffer with 10% sucrose, 10 mM Tris-maleate, and 0.9% NaCl, pH 6.8. Aliquots were snap-frozen in liquid N_2 and stored at −80°C until used.

NOS activity assay. RV and LV tissues were homogenized, and NOS activity was determined using the conversion of L-[^{3}H]arginine to L-[^{3}H]citrulline as previously described (25). All activities were normalized to the amount of protein in each lysate. To determine the potential contribution of iNOS to total NOS activity, assays were repeated without Ca^{2+} supplementation.

Statistical analysis. For Western blot protein analysis and NOS activity, data are shown as means ± SD. Quantitative PCR data are shown as means ± SE. ANOVA was used to compare differences in these parameters between the three groups with Bonferroni correction for multiple comparisons. A $P < 0.05$ was considered significant.

RESULTS

Characteristics of juvenile shunt and control lambs. There were no differences in gestational age at delivery or total body weight between shunt and control lambs (11.1 ± 1.6 vs. 12.8 ± 2.6 kg, respectively, $P = 0.24$). In shunt lambs compared with controls, both RV and LV and interventricular septum (LV + S) chamber weights were increased, relative to body weight (RV/body wt $2.5 \times 10^{-3} \pm 4.9 \times 10^{-4}$ vs. $1.3 \times 10^{-3} \pm 9.6 \times 10^{-5}$, respectively, $P < 0.001$; LV + S/body wt $6.1 \times 10^{-3} \pm 6.5 \times 10^{-4}$ vs. $3.3 \times 10^{-3} \pm 2.1 \times 10^{-4}$, respectively, $P < 0.001$). Thus, there is gross morphological evidence of global, biventricular hypertrophy in shunt lambs. At the conclusion of each study, the heart and vasculature of each

lamb were examined; there were no patent ductus arteriosi or foramina ovalia.

Hemodynamics of juvenile shunt and control lambs. As expected, shunt lambs had significantly higher pulmonary blood flow compared with control lambs (indexed left pulmonary artery blood flow: 175 ± 28.6 vs. 40.1 ± 16.4 ml·min^{-1}·kg body wt^{-1}, respectively; $P < 0.0001$). The ratio of pulmonary to systemic blood flow was 2.76 ± 0.7 in shunt lambs. Mean pulmonary artery pressures were also significantly elevated in shunt lambs compared with control lambs (24.7 ± 1.4 vs. 11.6 ± 3.0 mmHg, respectively, $P < 0.0001$). There were no significant differences between shunt and control lambs in heart rate or mean systemic systolic blood pressure (62 ± 5.6 vs. 68 ± 6.7 mmHg, respectively, $P = 0.8$). As expected, systemic diastolic blood pressure was significantly lower in shunt lambs compared with controls (30.3 ± 3.7 vs. 53.6 ± 4.1, respectively, $P < 0.001$).

NOS isoform expression. In examining NO-mediated signaling in the RV of shunt animals, we first investigated the expression of various NOS isoforms. Using qPCR, we quantified mRNA levels of eNOS, nNOS, and iNOS. The transcription of all three isoforms was greater in the RV of shunt and fetal lambs compared with control lambs (eNOS, 3.0 ± 1.0- and 4.9 ± 0.7-fold vs. control, respectively; nNOS 10.2 ± 4.9- and 25.3 ± 7.2-fold vs. control, respectively; iNOS 2.0 ± 0.7- and 3.2 ± 0.8-fold vs. control, respectively; $P < 0.05$, Fig. 1, *A–C*). The transcription of eNOS and nNOS was greater in the LV of fetal lambs compared with shunt and control lambs. Similarly, when we investigated protein expression of the various NOS isoforms, we found that protein expression of all three isoforms was greater in the RV of shunt and fetal lambs compared with control lambs (eNOS, 1.3- and 1.6-fold vs. control, respectively; nNOS 1.4 ± 0.1- and 1.6 ± 0.2-fold vs. control, respectively; iNOS 1.4 ± 0.1- and 1.7 ± 0.2-fold vs. control, respectively; $P < 0.05$, Fig. 1, *D–F*). The protein expression of all three isoforms was greater in the LV of fetal lambs compared with shunt and control lambs.

Immunohistochemistry. Because increased NOS isoform expression may be the result of multiple cell types within the

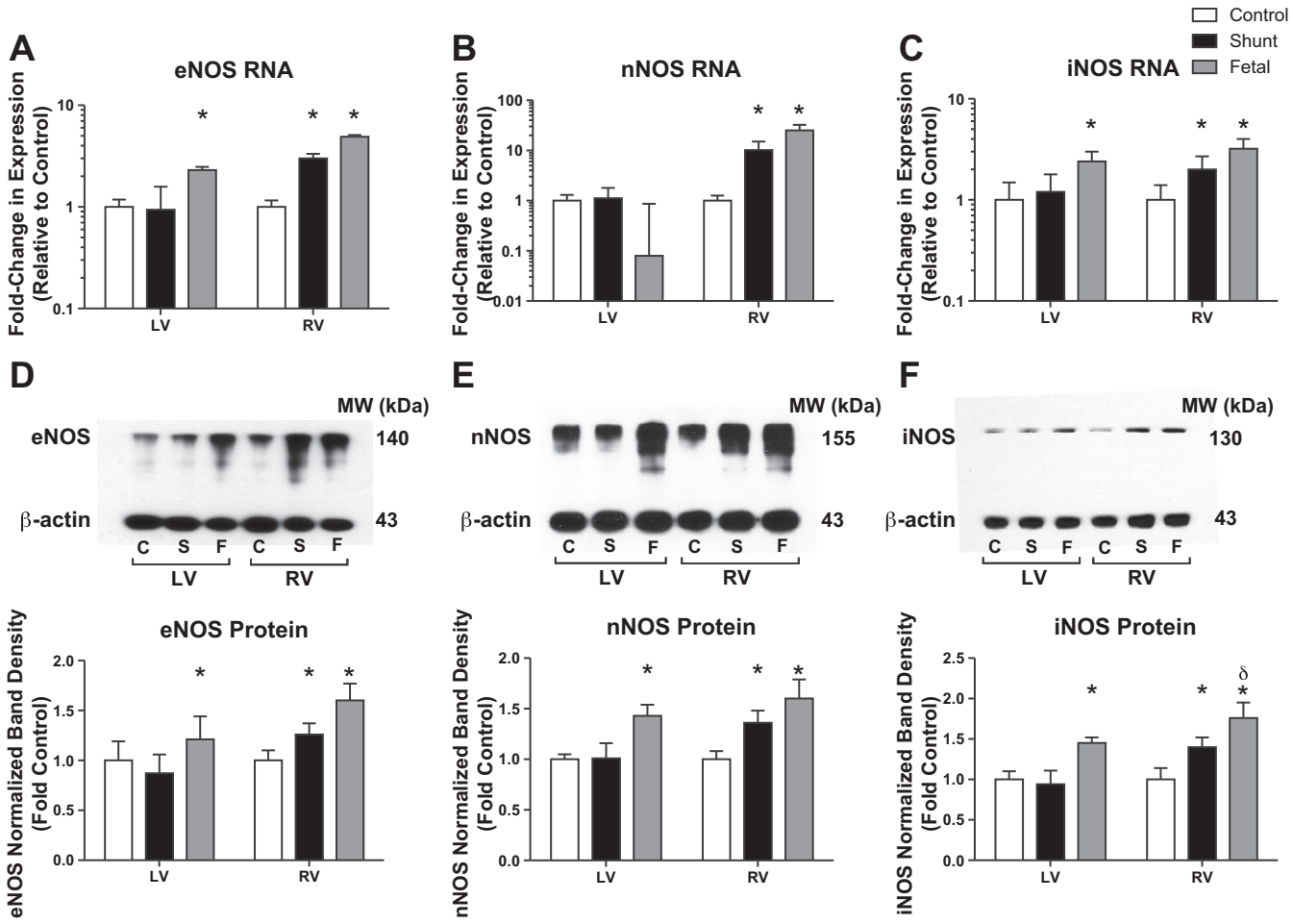

Fig. 1. Nitric oxide synthase (NOS) isoform expression. *A–C*: transcription of endothelial (eNOS, *A*), neuronal (nNOS, *B*), and inducible (iNOS, *C*) NOS RNA is upregulated in shunt and fetal right ventricle (RV) relative to control. There is no significant difference between shunt and fetal NOS isoform RNA expression. RNA expression was quantified by qPCR, and data are shown as means ± SE. *D–F*: protein expression of eNOS (*D*), nNOS (*E*), and iNOS (*F*) is upregulated in shunt and fetal RV relative to control. There are no differences in RV eNOS and nNOS expression between shunt and fetal groups; fetal RV iNOS expression is significantly greater than shunt RV iNOS expression. Protein expression was quantified by Western blot. For each isoform, immunoblots were performed on different membranes in parallel using identical aliquots of the same protein homogenate; $n = 5$ experiments in all groups. $P < 0.05$ compared with control (*) and shunt (δ). Immunoblots shown were performed using pooled samples for publication purposes only. The bar graphs and stated results represent densitometry performed on individual samples. LV, left ventricle; MW, molecular mass marker; C, control; S, shunt; F, fetal.

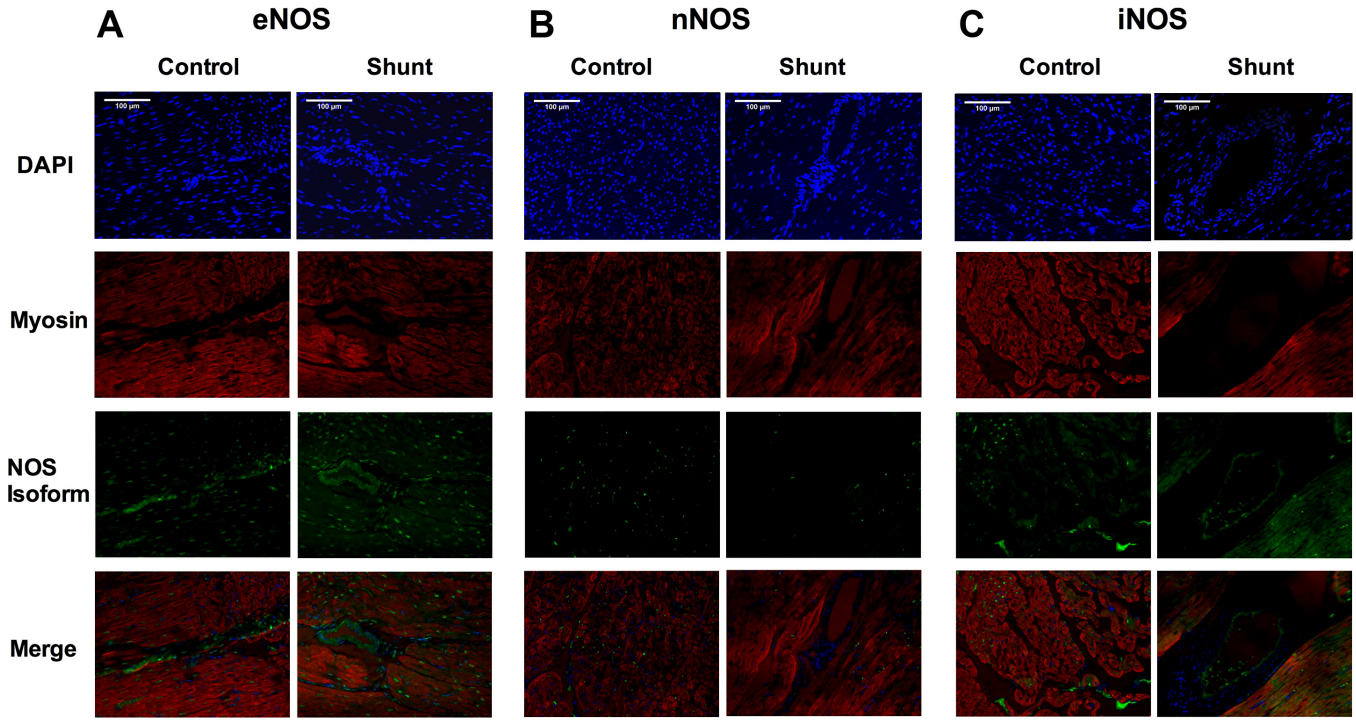

Fig. 2. Localization of NOS isoforms within control and shunt RV tissue. For each panel, control RV is on the *left*, and shunt RV is on the *right*. Stains are arranged vertically: *top*, 4′,6-diamidino-2-phenylindole (DAPI, blue); *top middle*, myosin (red); *bottom middle*, NOS isoform (green); *bottom*, merge. *A*: eNOS is localized within shunt RV cardiomyocyte cytoplasm and nuclei, whereas eNOS localizes only within cardiomyocyte nuclei in control RV. *B*: nNOS does not localize within cardiomyocytes in control RV tissue but does in shunt RV. *C*: iNOS localizes within cardiomyoctes in both control and shunt RV tissue.

ventricle, we then performed immunohistochemistry on serial RV sections obtained from shunt lambs to determine colocalization of NOS isoforms within cardiac tissue (Fig. 2). As expected, there was prominent localization of eNOS within endothelial cells found in myocardial capillaries in both shunt and control RV tissue. However, in shunt RV tissue, eNOS localizes to both the cardiomyocyte nucleus and cytoplasm; in control RV tissue, eNOS localization within the cardiomyocyte is confined to the nucleus (Fig. 2*A*). In control RV tissue, nNOS does not localize within the cardiomyocytes while in shunt RV tissue nNOS localizes within cardiomyocyte cytoplasm (Fig. 2*B*). Finally, iNOS appears to have some localization within the cardiomyocyte of both control and shunt RV tissue (Fig. 2*C*).

NOS activity. Having shown increased RNA transcription and protein expression of all three NOS isoforms in fetal and shunt RV compared with control, we next quantified NOS activity in these tissues. The assay distinguishes between total NOS activity and Ca^{+2}-independent activity, which is the result of iNOS alone. Total NOS activity was increased in the RV of shunt and fetal lambs compared with control lambs (2.5 ± 0.56- and 3.5 ± 0.37-fold vs. control, respectively; $P < 0.05$, Fig. 3*B*). In contrast, total NOS activity in the LV was not different between groups (Fig. 3*A*). Ca^{+2}-independent NOS activity in the RV and LV was not different between groups.

NOS regulation and signaling activity. After increased NOS expression and activity in shunt and fetal RV was established, we next sought to determine the relationship between NOS-associated signaling proteins and activating pathways. Using IP, we found increased association of eNOS with calmodulin in the RV of shunt and fetal lambs compared with controls (1.8 ± 0.2- and 1.5 ± 0.1-fold vs. control, respectively; $P < 0.05$, Fig. 4*A*). Although this association was increased in the LV of fetal lambs ($P < 0.05$), there were no differences between control and shunt lambs. We next examined the association of eNOS with hsp90. We found hsp90 to be more associated with

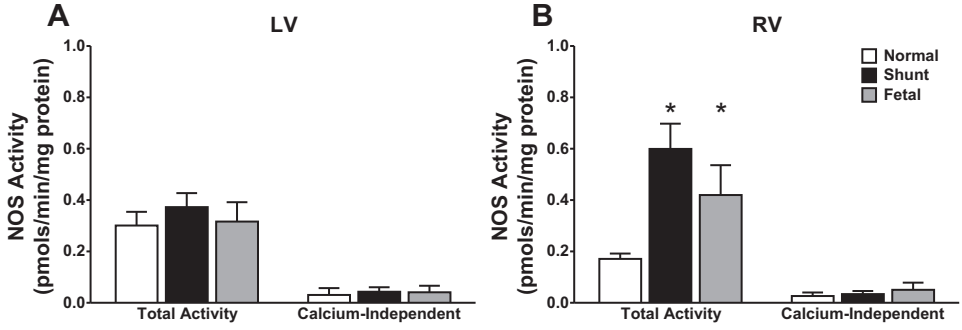

Fig. 3. Total NOS activity and Ca^{2+}-independent NOS activity in LV and RV tissue from control, shunt, and fetal lambs. *A*: in LV tissue, there were no differences in either total NOS activity or Ca^{2+}-independent NOS activity (iNOS activity). *B*: in RV tissue, both shunt and fetal lambs had increased total NOS activity compared with controls, but there were no differences between groups in Ca^{2+}-independent NOS activity; $n = 5$ in all groups. Values are means ± SD. *$P < 0.05$ compared with control.

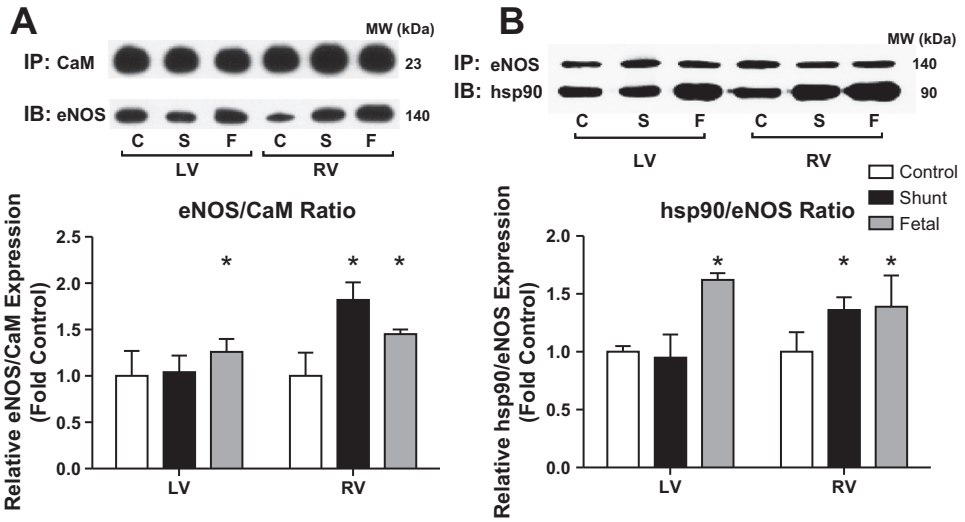

Fig. 4. eNOS association with allosteric modulator calmodulin and chaperone protein 90-kDa heat shock protein (hsp90). *A*: after immunoprecipitation (IP) using anticalmodulin (CaM) antibody, immunoblot (IB) was performed for eNOS. eNOS is significantly more associated with CaM in both shunt and fetal RV tissue compared with controls. eNOS levels were normalized to CaM protein after IP. *B*: after IP using anti-eNOS antibody, IB was performed for hsp90. The hsp90 is significantly more associated with eNOS in both shunt and fetal RV compared with controls. The hsp90 levels were normalized to eNOS protein after IP; $n = 5$ in all groups. Values are means ± SD. $^*P < 0.05$ compared with control. IBs shown were performed using pooled samples for publication purposes only. The bar graphs and stated results represent densitometry performed on individual samples.

eNOS in the RV of shunt and fetal lambs compared with controls (1.4 ± 0.1- and 1.4 ± 0.2-fold vs. control, respectively; $P < 0.05$, Fig. 4*B*). Although this association was also increased in the LV of fetal lambs ($P < 0.05$), there were no differences between control and shunt lambs.

Akt is a serine-threonine kinase that associates with the eNOS complex through interaction with hsp90, increasing eNOS activity by phosphorylating serine residue 1177 (1, 23). To better understand the importance of this pathway in the RV of shunt lambs, we first investigated Akt expression. We found both increased transcription of Akt mRNA (2.9 ± 0.3- and 4.1 ± 0.2-fold vs. control, respectively; $P < 0.05$, Fig. 5*A*) and Akt protein expression (2.1 ± 0.2- and 2.3 ± 0.2-fold vs. control, respectively; $P < 0.05$, Fig. 5*B*) in the RV of shunt and fetal

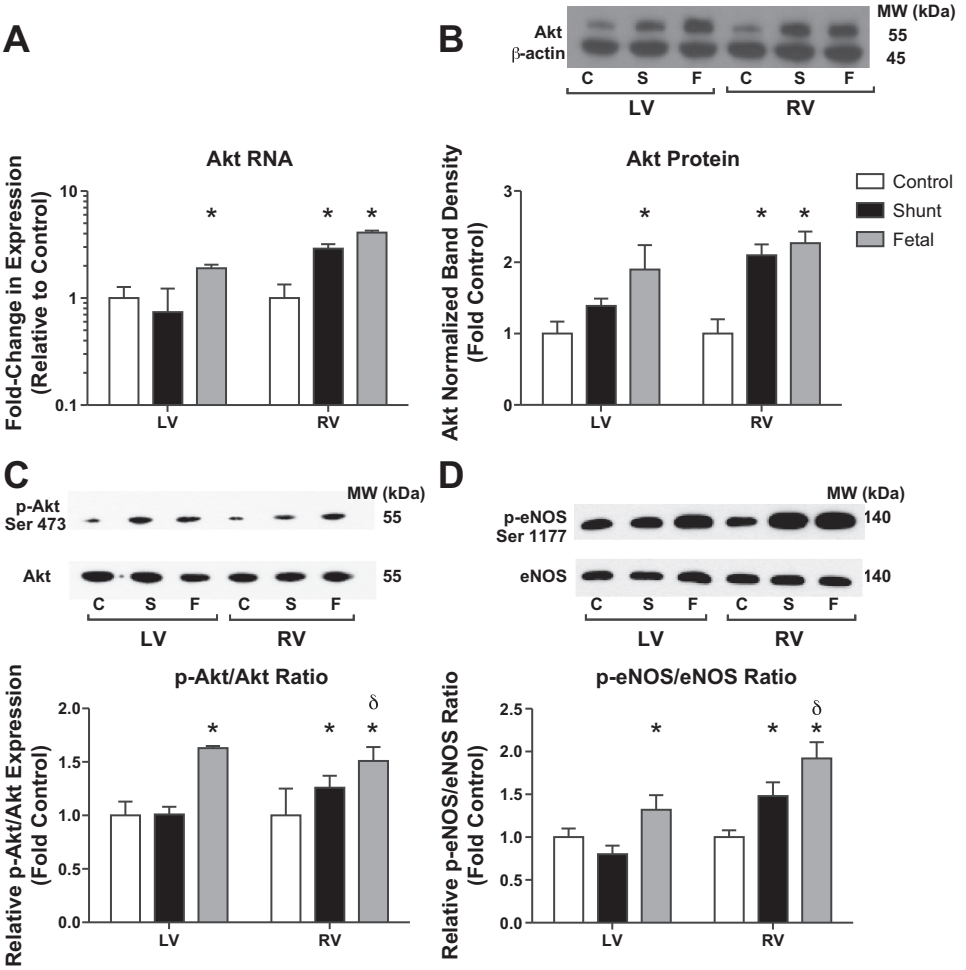

Fig. 5. Akt expression and phosphorylation and eNOS phosphorylation. *A*: transcription of Akt RNA is upregulated in shunt and fetal RV compared with control. Fetal LV has increased Akt RNA transcription, but there is no increase in shunt LV Akt RNA expression compared with control. Values are means ± SE. *B*: Akt protein expression is significantly increased in shunt and fetal RV tissue relative to control. Whereas fetal LV Akt protein expression is significantly increased, there is no change in shunt LV expression relative to control. Values are means ± SD. *C*: Akt phosphorylation is increased in shunt RV tissue relative to control, and an even greater proportion of fetal RV Akt is phosphorylated compared with both shunt and control. Fetal LV tissue also had increased Akt phosphorylation. IP was performed with Akt antibody, and then p-Akt protein was quantified and normalized to total Akt protein. Values are means ± SD. *D*: eNOS phosphorylation by Akt at serine residue 1177 is increased in shunt RV tissue relative to controls; Ser^{1177}-p-eNOS is further increased in fetal RV tissue compared with both shunt and control. Fetal LV tissue also has significantly greater Ser^{1177}-p-eNOS relatively to control, but there are no differences in shunt and control LV. Values are means ± SD; $n = 5$ in all groups. $P < 0.05$ compared with control (*) and shunt (δ). IBs shown were performed using pooled samples for publication purposes only. The bar graphs and stated results represent densitometry performed on individual samples.

lambs compared with controls. Although Akt expression was increased in the LV of fetal lambs ($P < 0.05$), there were no differences between control and shunt lambs (Fig. 5*B*). Next, we found greater Akt phosphorylation in the RV of shunt and fetal lambs compared with controls; however, the p-Akt proportion was even greater in fetal RV tissue compared with shunt (1.3 ± 0.1- and 1.5 ± 0.1-fold vs. control, respectively; $P < 0.05$, Fig. 5*C*). We found greater Akt phosphorylation in the LV of fetal lambs compared with shunt and control lambs (with no differences between shunt and control). Last, we examined Akt activation of eNOS by quantifying the proportion of eNOS phosphorylated at the serine-1177 residue (Ser^{1177}-p-eNOS). We found greater Ser^{1177}-p-eNOS in the RV of shunt and fetal lambs compared with controls; however, the proportion was even greater in fetal than shunt lambs (1.9 ± 0.2- and 1.5 ± 0.2-fold vs. control, respectively; $P < 0.05$, Fig. 5*D*). In the LV, Ser^{1177}-p-eNOS was greater in fetal lambs compared with shunt and control lambs ($P < 0.05$).

RyR2 is a Ca^{2+} release channel located at the SR and a vital part of excitation-contraction coupling (30). Posttranslational modification of RyR2 via *S*-nitrosylation (SNO) of cysteine residues increases the open probability of RyR2 channels, thus increasing Ca^{2+} transient in cardiomyocytes and increasing contractility. Using IP for RyR2, we then examined the portion of RyR2 with SNO modification. We found greater RyR2-SNO proportion in the RV of shunt and fetal lambs compared with controls; however, the proportion was even greater in fetal than shunt lambs (1.4 ± 0.16- and 1.9 ± 0.08-fold vs. control, respectively, $P < 0.05$, Fig. 6). In the LV, the RyR2-SNO proportion was greater in fetal lambs compared with shunt and control lambs ($P < 0.05$).

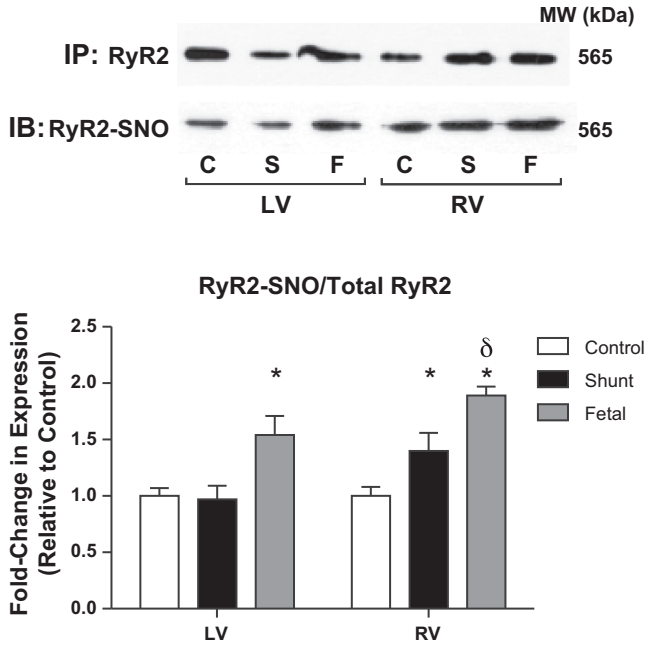

Fig. 6. Ryanodine receptor 2 (RyR2) modification by *S*-nitrosylation (SNO). After isolation of sarcoplasmic reticulum vesicles, IP was performed for RyR2, and then IB was performed for SNO at the appropriate molecular weight for RyR2. A more significant proportion of RyR2 exists in nitrosylated form in both shunt and fetal RV compared with controls; $n = 5$ in all groups. Values are means ± SD. $P < 0.05$ compared with control (*) and shunt (δ). IBs shown were performed using pooled samples for publication purposes only. The bar graphs and stated results represent densitometry performed on individual samples.

DISCUSSION

In fetal circulation, the RV accounts for the majority of cardiac output (24, 33), and the fetal RV is more resilient to physiological stress, such as acidosis and hypoxia, compared with the fetal LV (20). During the transition to postnatal circulation, the RV remodels to a thin-walled, compliant ventricle coupled to a low-impendence pulmonary vascular system. After this transition is complete, the RV is unable to effectively or efficiently respond to increases in afterload, which may be due to loss of the protective structural and molecular fetal phenotype (9). Conversely, in CHD with a posttricuspid level shunt, this normal postnatal transition is delayed and abrogated; for example, the attenuated fall in pulmonary vascular resistance and pulmonary artery pressure after birth in patients with a large ventricular septal defect is well described (28). Although the effects of this altered transition in CHD on RV function and remodeling are unclear, patient case series suggest that normal regression of RV wall thickness does not occur in patients with CHD who ultimately develop Eisenmenger's syndrome (16). Consequently, these patients with PH associated with CHD have better functional ability and improved survival compared with patients with primary PH (15, 22). Interestingly, among patients with primary PH, there is considerable variability in indexes of RV function (cardiac output and right atrial pressure) relative to pulmonary artery pressure elevation. There is a subpopulation of patients who retain an adaptive phenotype with concentric hypertrophy and preserved mechanical efficiency; accordingly, these patients have improved survival compared with patients with a "maladaptive" RV phenotype (4). The importance of RV function in both PH and CHD is gaining recognition, but the mechanisms underlying the adaptive RV phenotype are unclear and yet may represent targets for novel therapies.

To this end, the current study used a clinically relevant lamb model of CHD with a large, unrestrictive aortopulmonary shunt placed during fetal life. Importantly, such a shunt does not change fetal hemodynamics but mimics the physiology of patients with CHD (with systemic-to-pulmonary shunts) during the transition from fetal to postnatal circulation. We demonstrated previously that shunt lambs have superior cardiac performance in response to acute increases in RV afterload because of the Anrep effect (19). Thus, this fetal model is ideal for investigations into underlying mechanisms for RV adaptation. The signaling mechanisms of the LV Anrep effect are well described and implicate a pivotal role for LV NO signaling (5, 10). Therefore, we focused this investigation on potential alterations in cardiac NO signaling.

Increased cardiac NO signaling has a variety of paracrine and autocrine effects that ultimately maximize cardiac function: dilation of coronary arteries with enhanced oxygen delivery, increased angiogenesis in hypertrophy, increased lusitropy with optimization of diastolic reserve, and improved excitation-contraction coupling that is crucial for the Anrep effect (5). To our knowledge, the studies presented herein are

the first to describe a unique RV NO signaling phenotype. In these investigations, we found a distinct RV shunt phenotype (compared with the shunt LV) with consistently increased NOS expression, activity, and association of important cofactors for NOS activation.

We first demonstrated increased expression of all NOS isoforms in the RV of shunt and fetal lambs; eNOS and nNOS are the most important isoforms, since they are constitutively expressed in cardiomyocytes. Both eNOS and nNOS isoforms have been implicated in single myocyte experiments as critical mediators of the Anrep effect (18, 31). Although we also found increased iNOS expression, the importance of this finding is less clear. The NOS activity assay demonstrated low levels of Ca^{2+}-independent NOS activity, attributable to iNOS; furthermore, there were no differences in Ca^{2+}-independent activity between control, shunt, and fetal lambs in either ventricle. However, total NOS activity was significantly increased in the RV of both shunt and fetal animals, reflecting important functional consequences of increased protein expression of eNOS and nNOS.

Although iNOS expression is increased in the RV of shunt and fetal lambs compared with control lambs we found no increase in iNOS-derived Ca^{2+}-independent NOS activity. iNOS-derived NO production is known to contribute to increase reactive oxygen species and inhibit Ca^{2+}-independent NOS activity (11); conversely, maintenance of the eNOS-to-iNOS expression ratio is known to suppress iNOS-derived NO production (14). Given that protein expression of all three NOS isoforms is increased to a similar extent, there are no significant changes in the eNOS-to-iNOS ratio between groups; this may account for the low level of Ca^{2+}-independent NOS activity seen in all three groups, since iNOS-derived NO production is inhibited under basal conditions.

Beyond increased expression and total activity, the shunt and fetal RV had a global picture of increased NOS activation. In each case, there was greater eNOS association with critical cofactors calmodulin and hsp90, which increase NOS activity (2, 7). Ca^{+2}-calmodulin binding to the eNOS complex is critical for disruption of inhibiting interactions with eNOS and also promotes allosteric modification of eNOS to derepress reductase catalytic activity to proceed (13). hsp90 likely increases NOS activity through two mechanisms, increasing the affinity of NOS for Ca^{+2}-calmodulin,(7) and recruiting Akt to the NOS complex and preventing its inactivation via dephosphylation (12, 31). Furthermore, Akt expression, activation, and phosphorylation of eNOS on serine residue 1177 were similarly upregulated. These findings may be because of stretch-mediated mechanisms of progressive NOS activation that were recently reviewed (5). The RV of shunts is likely also subject to these stretch-mediated mechanisms given significantly increased end-diastolic, end-systolic, and overall stroke volumes seen in the RV of shunt lambs compared with control (19).

nNOS has also been implicated as a critical mediator of excitation-contraction coupling, partly through reversible nitrosylation of cysteine residues on RyR2, a crucial Ca^{2+} channel on the SR. RyR2 exists as a tetramer and is progressively activated by nitrosylation of thiol groups, with maximal activation (2- to 3-fold baseline) achieved when approximately three thiol groups per subunit are nitrosylated (32). nNOS localizes to the SR, making it the most likely NOS isoform responsible for RyR2 nitrosylation (6). Furthermore, myocytes derived from nNOS knockout mice have decreased RyR2 activity, a phenotype that can be rescued through addition of *S*-nitroso-*N*-acetyl-DL-penicillamine, an NO donor and nitrosylating agent (30). In the current study, we have demonstrated increased expression of nNOS RNA and protein and increased nitrosylation of RyR2 in SR vesicles isolated from shunt and fetal RV tissue; this provides a possible mechanism underlying our earlier observation of superior cardiac performance in the RV of shunt lambs (19).

In this study, we demonstrated increased NO signaling from increased isoform expression and total NOS activity as well as signaling associated with both eNOS and nNOS. However, NO signaling in cardiovascular physiology and pathology is complex, with NO production having differing and even opposing effects depending on subcellular localization and production. The precise physiological effects of these observations and the effects of increased NO activity on physical properties such as angiogenesis and the development of ventricular hypertrophy are crucial matters for further investigation.

Perhaps the most intriguing finding of the current study was the consistent pattern of NOS expression and activation between the RV of shunt and fetal lambs. Although not identical, the alterations in shunt and fetal RV expression compared with control lambs were remarkably similar. The current investigation into shunt and fetal RV expression was necessarily limited, but these data strongly support our hypothesis that the hemodynamic stimulus of an unrestrictive systemic-to-pulmonary shunt at the time of birth attenuates the normal transition from a fetal RV phenotype and that these preserved fetal characteristics confer a physiological advantage. A more global investigation of expression similarities and dissimilarities between shunt and fetal RV is necessary to further explore this hypothesis.

The most important limitation of this study was that we did not test the functional implications of the observed increases in NO signaling. An important next area of investigation will be pharmacological modulation of the NO pathway in both isolated cardiac and whole animal preparations to recapitulate the observed physiological adaptations we found in the RV of shunted animals. However, the current findings provide important foundational work for these studies.

In summary, our findings of increased NOS expression and activity in the RV of shunt and fetal lambs taken together with our physiological observations suggest a potentially crucial role for NO signaling in the adaptive RV response to increased afterload under conditions of chronic (since birth) left-to-right shunting. In almost all other animal models of either PH or CHD, the RV suffers maladaptive hypertrophy with progression to RV failure. In contrast, insights gained from this model with an adaptive physiological response may ultimately point to innovative therapeutic strategies. For example, the current finding of increased RV NO signaling, if validated to have advantageous physiological consequences, has clear potential therapeutic implications, since many existing PH therapies target the NO pathway. Furthermore, these findings lend further support to the hypothesis that patients with certain types of CHD have a preserved, advantageous fetal phenotype that

may ultimately lead to previously overlooked strategies in treating all patients with RV failure in PH and CHD.

ACKNOWLEDGMENTS

We thank Linda Talken and the University of California Davis Veterinary Staff for excellent animal care.

GRANTS

This research was supported in part by grants from the National Institutes of Health (HL-61284 to J. R. Fineman and 5T32-HD-049303-07 to J. R. Fineman and R. J. Kameny) and the American Heart Association (14FTF19670001 to R. J. Kameny).

DISCLOSURES

The authors have no conflict of interests to disclose.

AUTHOR CONTRIBUTIONS

Author contributions: R.J.K., S.A.D., P.E.O., and J.R.F. conception and design of research; R.J.K., Y.H., C.M., C.E.S., M.J.J., W.G., and G.W.R. performed experiments; R.J.K., Y.H., C.M., and C.E.S. analyzed data; R.J.K., Y.H., S.A.D., P.E.O., and J.R.F. interpreted results of experiments; R.J.K. and C.E.S. prepared figures; R.J.K. drafted manuscript; R.J.K., P.E.O., and J.R.F. edited and revised manuscript; R.J.K., Y.H., C.M., C.E.S., M.J.J., W.G., G.W.R., S.A.D., P.E.O., and J.R.F. approved final version of manuscript.

REFERENCES

1. **Adak S, Santolini J, Tikunova S, Wang Q, Johnson JD, Stuehr DJ.** Neuronal nitric-oxide synthase mutant (Ser-1412 → Asp) demonstrates surprising connections between heme reduction, NO complex formation, and catalysis. *J Biol Chem* 276: 1244–1252, 2001.
2. **Azakie A, Fineman J, He Y.** Differential responses of the right ventricle to abnormal loading conditions in vivo: possible pathophysiologic mechanisms. *J Thorac Cardiovasc Surg* 145: 1335–1344, 2013.
3. **Azakie A, Fineman JR, He Y.** Sp3 inhibits Sp1-mediated activation of the cardiac troponin T promoter and is downregulated during pathological cardiac hypertrophy in vivo. *Am J Physiol Heart Circ Physiol* 291: H600–H611, 2006.
4. **Badagliacca R, Poscia R, Pezzuto B, Nocioni M, Mezzapesa M, Francone M, Giannetta E, Papa S, Gambardella C, Sciomer S, Volterrani M, Fedele F, Dario Vizza C.** Right ventricular remodeling in idiopathic pulmonary arterial hypertension: adaptive versus maladaptive morphology. *J Heart Lung Transplant* 34: 395–403, 2015.
5. **Balligand JL, Feron O, Dessy C.** eNOS activation by physical forces: from short-term regulation of contraction to chronic remodeling of cardiovascular tissues. *Physiol Rev* 89: 481–534, 2009.
6. **Barouch LA, Harrison RW, Skaf MW, Rosas GO, Cappola TP, Kobeissi ZA, Hobai IA, Lemmon CA, Burnett AL, O'Rourke B, Rodriguez ER, Huang PL, Lima JAC, Berkowitz DE, Hare JM.** Nitric oxide regulates the heart by spatial confinement of nitric oxide synthase isoforms. *Nature* 416: 337–339, 2002.
7. **Bender AT, Silverstein AM, Demady DR, Kanelakis KC, Noguchi S, Pratt WB, Osawa Y.** Neuronal nitric-oxide synthase is regulated by the Hsp90-based chaperone system in vivo. *J Biol Chem* 274: 1472–1478, 1999.
8. **Buck ED, Lachnit WG, Pessah IN.** Mechanisms of delta-hexachlorocyclohexane toxicity: I. Relationship between altered ventricular myocyte contractility and ryanodine receptor function. *J Pharmacol Exp Ther* 289: 477–485, 1999.
9. **Chin KM, Kim NHS, Rubin LJ.** The right ventricle in pulmonary hypertension. *Coron Artery Dis* 16: 13–18, 2005.
10. **Cingolani HE, Perez NG, Cingolani OH, Ennis IL.** The Anrep effect: 100 years later. *Am J Physiol Heart Circ Physiol* 304: H175–H182, 2013.
11. **Csiszar A, Ungvari Z, Edwards JG, Kaminski P, Wolin MS, Koller A, Kaley G.** Aging-induced phenotypic changes and oxidative stress impair coronary arteriolar function. *Circ Res* 90: 1159–1166, 2002.
12. **Fontana J, Fulton D, Chen Y, Fairchild TA, McCabe TJ, Fujita N, Tsuruo T, Sessa WC.** Domain mapping studies reveal that the M domain of hsp90 serves as a molecular scaffold to regulate Akt-dependent phosphorylation of endothelial nitric oxide synthase and NO release. *Circ Res* 90: 866–873, 2002.
13. **Garcin ED, Bruns CM, Lloyd SJ, Hosfield DJ, Tiso M, Gachhui R, Stuehr DJ, Tainer JA, Getzoff ED.** Structural basis for isozyme-specific regulation of electron transfer in nitric-oxide synthase. *J Biol Chem* 279: 37918–37927, 2004.
14. **Gong X, Ma Y, Ruan Y, Fu G, Wu S.** Long-term atorvastatin improves age-related endothelial dysfunction by ameliorating oxidative stress and normalizing eNOS/iNOS imbalance in rat aorta. *Exp Gerontol* 52: 9–17, 2014.
15. **Hopkins WE, Ochoa LL, Richardson GW, Trulock EP.** Comparison of the hemodynamics and survival of adults with severe primary pulmonary hypertension or Eisenmenger syndrome. *J Heart Lung Transplant* 15: 100–105, 1996.
16. **Hopkins WE, Waggoner AD.** Severe pulmonary hypertension without right ventricular failure: the unique hearts of patients with Eisenmenger syndrome. *Am J Cardiol* 89: 34–38, 2002.
17. **Hopkins WE.** The remarkable right ventricle of patients with Eisenmenger syndrome. *Coron Artery Dis* 16: 19–25, 2005.
18. **Jian Z, Han H, Zhang T, Puglisi J, Izu LT, Shaw JA, Onofiok E, Erickson JR, Chen YJ, Horvath B, Shimkunas R, Xiao W, Li Y, Pan T, Chan J, Banyasz T, Tardiff JC, Chiamvimonvat N, Bers DM, Lam KS, Chen-Izu Y.** Mechanochemotransduction during cardiomyocyte contraction is mediated by localized nitric oxide signaling. *Sci Signal* 7: 7–27, 2014.
19. **Johnson RC, Datar SA, Oishi PE, Bennett S, Maki J, Sun C, Johengen M, He Y, Raff GW, Redington AN, Fineman JR.** Adaptive right ventricular performance in response to acutely increased afterload in a lamb model of congenital heart disease: evidence for enhanced Anrep effect. *Am J Physiol Heart Circ Physiol* 306: H1222–H1230, 2014.
20. **Junno J, Bruun E, Gutierrez JH, Erkinaro T, Haapsamo M, Acharya G, Räsänen J.** Fetal sheep left ventricle is more sensitive than right ventricle to progressively worsening hypoxemia and acidemia. *Eur J Obstet Gynecol Reprod Biol* 167: 137–141, 2013.
21. **Livak KJ, Schmittgen TD.** Analysis of relative gene expression data using real-time quantitative PCR and the 2(-Delta Delta C(T)) method. *Methods* 25: 402–408, 2001.
22. **McLaughlin VV, Archer SL, Badesch DB, Barst RJ, Farber HW, Lindner JR, Mathier MA, McGoon MD, Park MH, Rosenson RS, Rubin LJ, Tapson VF, Varga J, Harrington RA, Anderson JL, Bates ER, Bridges CR, Eisenberg MJ, Ferrari VA, Grines CL, Hlatky MA, Jacobs AK, Kaul S, Lichtenberg RC, Moliterno DJ, Mukherjee D, Pohost GM, Schofield RS, Shubrooks SJ, Stein JH, Tracy CM, Weitz HH, Wesley DJ, ACCF/AHA.** ACCF/AHA 2009 expert consensus document on pulmonary hypertension: a report of the American College of Cardiology Foundation Task Force on Expert Consensus Documents and the American Heart Association: developed in collaboration with the American College of Chest Physicians, American Thoracic Society, and the Pulmonary Hypertension Association. *Circulation* 120: 2250–2294, 2009.
23. **Michell BJ, Griffiths JE, Mitchelhill KI, Rodriguez-Crespo I, Tiganis T, Bozinovski S, de Montellano PR, Kemp BE, Pearson RB.** The Akt kinase signals directly to endothelial nitric oxide synthase. *Curr Biol* 9: 845–848, 1999.
24. **Mielke G, Benda N.** Cardiac output and central distribution of blood flow in the human fetus. *Circulation* 103: 1662–1668, 2001.
25. **Oishi PE, Wiseman DA, Sharma S, Kumar S, Hou Y, Datar SA, Azakie A, Johengen MJ, Harmon C, Fratz S, Fineman JR, Black SM.** Progressive dysfunction of nitric oxide synthase in a lamb model of chronically increased pulmonary blood flow: a role for oxidative stress. *Am J Physiol Lung Cell Mol Physiol* 295: L756–L766, 2008.
26. **Petroff MG, Kim SH, Pepe S, Dessy C, Marbán E, Balligand JL, Sollott SJ.** Endogenous nitric oxide mechanisms mediate the stretch dependence of Ca2+ release in cardiomyocytes. *Nat Cell Biol* 3: 867–873, 2001.
27. **Reddy VM, Meyrick B, Wong J, Khoor A, Liddicoat JR, Hanley FL, Fineman JR.** In utero placement of aortopulmonary shunts. A model of postnatal pulmonary hypertension with increased pulmonary blood flow in lambs. *Circulation* 92: 606–613, 1995.
28. **Rudolph AM.** Circulatory adjustments after birth: effects on ventricular septal defect. *Br Heart J* 33: 32–34, 1971.
29. **Sears CE, Bryant SM, Ashley EA, Lygate CA, Rakovic S, Wallis HL, Neubauer S, Terrar DA, Casadei B.** Cardiac neuronal nitric oxide synthase isoform regulates myocardial contraction and calcium handling. *Circ Res* 92: e52–e59, 2003.

30. **Wang H, Viatchenko-Karpinski S, Sun J, Györke I, Benkusky NA, Kohr MJ, Valdivia HH, Murphy E, Györke S, Ziolo MT.** Regulation of myocyte contraction via neuronal nitric oxide synthase: role of ryanodine receptor S-nitrosylation. *J Physiol* 588: 2905–2917, 2010.
31. **Wei Q, Xia Y.** Roles of 3-phosphoinositide-dependent kinase 1 in the regulation of endothelial nitric-oxide synthase phosphorylation and function by heat shock protein 90. *J Biol Chem* 280: 18081–18086, 2005.
32. **Xu L, Eu JP, Meissner G, Stamler JS.** Activation of the cardiac calcium release channel (ryanodine receptor) by poly-S-nitrosylation. *Science* 279: 234–237, 1998.
33. **Zhou YQ, Cahill LS, Wong MD, Seed M, Macgowan CK, Sled JG.** Assessment of flow distribution in the mouse fetal circulation at late gestation by high-frequency Doppler ultrasound. *Physiol Genomics* 46: 602–614, 2014.